

Effects of Sodium Cationization vs. Protonation on the Conformations and N-Glycosidic

Bond Stabilities of Sodium Cationized Uridine and 2'-Deoxyuridine:

Solution Conformation of $[Urd+Na]^+$ is Preserved Upon ESI

**Y. Zhu[†], H. A. Roy[†], N. A. Cunningham[†], S. F. Strobehn[†], J. Gao[‡], M. U. Munshi[‡],
G. Berden[‡], J. Oomens[‡], and M. T. Rodgers^{†, *}**

[†]*Department of Chemistry, Wayne State University, Detroit, MI, 48202*

[‡]*Radboud University, Institute for Molecules and Materials, FELIX Laboratory, Toernooiveld 7c,
6525ED Nijmegen, The Netherlands*

Table S1. Mass List of Protonated and Sodium Cationized Urd and dUrd

m/z	Symbol	$[Urd+H]^+$	$[dUrd+H]^+$	$[Urd+Na]^+$	$[dUrd+Na]^+$
267.0	●	—	—	$[Urd+Na]^+$	—
251.0	●	—	—	—	$[dUrd+Na]^+$
245.0	●	$[Urd+H]^+$	—	—	—
229.0	●	—	$[dUrd+H]^+$	—	—
227.0	●	$[Urd-W+H]^+$	—	—	—
211.0	●	—	$[dUrd-W+H]^+$	—	—
203.0	●	$[Urd-K+H]^+$	—	—	—
193.0	●	—	$[dUrd-2W+H]^+$	—	—
185.0	●	$[Urd-K-W+H]^+$	—	—	—
155.0	●	—	—	$[Urd-Ura+Na]^+$	—
139.0	●	—	—	—	$[dUrd-Ura+Na]^+$
135.0	●	—	—	$[Ura+Na]^+$	$[Ura+Na]^+$
131.0	●	—	$[Ura+W+H]^+$	—	—
117.0	●	—	$[dUrd-Ura+H]^+$	—	—
113.0	●	$[Ura+H]^+$	$[Ura+H]^+$	—	—
99.0	●	—	$[dUrd-Ura-W+H]^+$	—	—
81.0	●	—	$[dUrd-Ura-2W+H]^+$	—	—

Table S2. Relative Gibbs Free Energies of the B3LYP/6-311+G(d,p) Optimized Structures of the T1(O2O4'05') and B1(O2O2') Conformers of $[\text{Urd}+\text{Na}]^+$ and Their Water Adducts ($[\text{Urd}+\text{Na}]^+ \cdot n\text{W}$, $n=1, 2$) Calculated Using Different Computational Approaches.^a

$[\text{Urd}+\text{Na}]^+$	B3LYP		MP2(full)	
	6-311+G(2d,2p)	def2-TZVPPD	6-311+G(2d,2p)	def2-TZVPPD
T1(O2O4'05')	0.0	0.0	0.0	0.0
B1(O2O2')	6.1	4.5	9.5	9.6
T1(O2O4'05')•W	1.6	3.1	0.0	0.0
B1(O2O2')•W	0.0	0.0	4.1	4.1
T1(O2O4'05')•2W	3.9	13.4	1.2	0.0
B1(O2O2')•2W	0.0	0.0	0.0	0.0

^aAll values are given in kJ/mol.

Table S3. Relative Gibbs Free Energies of the B3LYP/6-311+G(d,p) Optimized Structures of the T1, T2, T3 and T4(O2O4'05') Conformers of $[\text{dUrd}+\text{Na}]^+$ Calculated Using Different Computational Approaches.^a

$[\text{dUrd}+\text{Na}]^+$	B3LYP		MP2(full)	
	6-311+G(2d,2p)	def2-TZVPPD	6-311+G(2d,2p)	def2-TZVPPD
T1(O2O4'05')	0.0	0.0	0.0	0.0
T2(O2O4'05')	3.5	3.3	2.9	3.7
T3(O2O4'05')	5.5	5.0	1.5	1.9
T4(O2O4'05')	7.5	7.2	6.1	4.9

^aAll values are given in kJ/mol.

Figure Captions

Figure S1. Designations for nucleobase orientation and pseudorotation phase angle (P) of nucleosides. The pseudorotation phase angle, P , is calculated using eq (S1). E and T forms alternate every 18° .

$$\tan P = \frac{(v_4 + v_1) - (v_3 + v_0)}{2 \times v_2 \times (\sin 36^\circ + \sin 72^\circ)} \quad (\text{S1})$$

The angles, v_0 , v_1 , v_2 , v_3 and v_4 , represent the $\angle C4' O4' C1' C2'$, $\angle O4' C1' C2' C3'$, $\angle C1' C2' C3' C4'$, $\angle C2' C3' C4' O4'$ and $\angle C3' C4' O4' C1'$, respectively. In the upper section of the diagram, $v_2 > 0$, whereas in the lower section of the diagram, $v_2 < 0$. The combination of P and v_2 are used to identify the sugar puckering. If $v_2 > 0$, $P = P$; if $v_2 < 0$ $P \rightarrow P + 180^\circ$.

Figure S2. The mass spectra of MS^3 experiments of $[\text{dUrd}-\text{W}+\text{H}]^+$, $[\text{dUrd}-2\text{W}+\text{H}]^+$, $[\text{dUrd}-\text{Ura}+\text{H}]^+$ and $[\text{Urd}-\text{K}+\text{H}]^+$.

Figure S3. Stable low-energy conformers of $[\text{Urd}+\text{Na}]^+$. The Na^+ binding modes, orientations of uracil, sugar puckering, and the relative 298 K Gibbs free energies at the B3LYP/6-311+G(2d,2p)//B3LYP/6-311+G(d,p) level of theory are also listed for each structure.

Figure S4. Stable low-energy conformers of $[\text{dUrd}+\text{Na}]^+$. The Na^+ binding modes, orientations of uracil, sugar puckering, and the relative 298 K Gibbs free energies at the B3LYP/6-311+G(2d,2p)//B3LYP/6-311+G(d,p) level of theory are also listed for each structure.

Figure S5. Comparison of the experimental IRMPD action spectrum of $[\text{Urd}+\text{Na}]^+$ with the B3LYP/6-311+G(d,p) optimized structures and calculated linear IR spectra for *syn* oriented O2 binding conformers with spectral misalignments shaded in red. The B3LYP/6-311+G(2d,2p) relative Gibbs free energies at 298 K is also shown.

Figure S6. Comparison of the experimental IRMPD action spectrum of $[\text{Urd}+\text{Na}]^+$ with the B3LYP/6-311+G(d,p) optimized structures and calculated linear IR spectra for *anti* oriented O2 binding conformers with spectral misalignments shaded in red. The B3LYP/6-311+G(2d,2p) relative Gibbs free energies at 298 K is also shown.

Figure S7. Comparison of the experimental IRMPD action spectrum of $[\text{Urd}+\text{Na}]^+$ with the B3LYP/6-311+G(d,p) optimized structures and calculated linear IR spectra for O4 binding conformers with spectral misalignments shaded in red. The B3LYP/6-311+G(2d,2p) relative Gibbs free energies at 298 K is also shown.

Figure S8. Comparison of the experimental IRMPD action spectrum of $[\text{Urd}+\text{Na}]^+$ with the B3LYP/6-311+G(d,p) optimized structures and calculated linear IR spectra for sugar binding conformers with spectral misalignments shaded in red. The B3LYP/6-311+G(2d,2p) relative Gibbs free energies at 298 K is also shown.

Figure S9. Comparison of the experimental IRMPD action spectrum of $[\text{Urd}+\text{Na}]^+$ with the B3LYP/6-311+G(d,p) optimized structures and calculated linear IR spectra for tautomeric conformers with spectral misalignments shaded in red. The B3LYP/6-311+G(2d,2p) relative Gibbs free energies at 298 K is also shown.

Figure S10. Comparison of the experimental IRMPD action spectrum of $[\text{dUrd}+\text{Na}]^+$ with the B3LYP/6-311+G(d,p) optimized structures and calculated linear IR spectra for T(O2O4'O5') conformers with spectral misalignments shaded in red. The B3LYP/6-311+G(2d,2p) relative Gibbs free energies at 298 K is also shown.

Figure S11. Comparison of the experimental IRMPD action spectrum of $[dUrd+Na]^+$ with the B3LYP/6-311+G(d,p) optimized structures and calculated linear IR spectra for bidentate and monodentate O2 binding conformers with spectral misalignments shaded in red. The B3LYP/6-311+G(2d,2p) relative Gibbs free energies at 298 K is also shown.

Figure S12. Comparison of the experimental IRMPD action spectrum of $[dUrd+Na]^+$ with the B3LYP/6-311+G(d,p) optimized structures and calculated linear IR spectra for O4 binding conformers with spectral misalignments shaded in red. The B3LYP/6-311+G(2d,2p) relative Gibbs free energies at 298 K is also shown.

Figure S13. Comparison of the experimental IRMPD action spectrum of $[dUrd+Na]^+$ with the B3LYP/6-311+G(d,p) optimized structures and calculated linear IR spectra for sugar binding conformers with spectral misalignments shaded in red. The B3LYP/6-311+G(2d,2p) relative Gibbs free energies at 298 K is also shown.

Figure S14. Comparison of the experimental IRMPD action spectrum of $[dUrd+Na]^+$ with the B3LYP/6-311+G(d,p) optimized structures and calculated linear IR spectra for tautomeric conformers with spectral misalignments shaded in red. The B3LYP/6-311+G(2d,2p) relative Gibbs free energies at 298 K is also shown.

Figure S1.

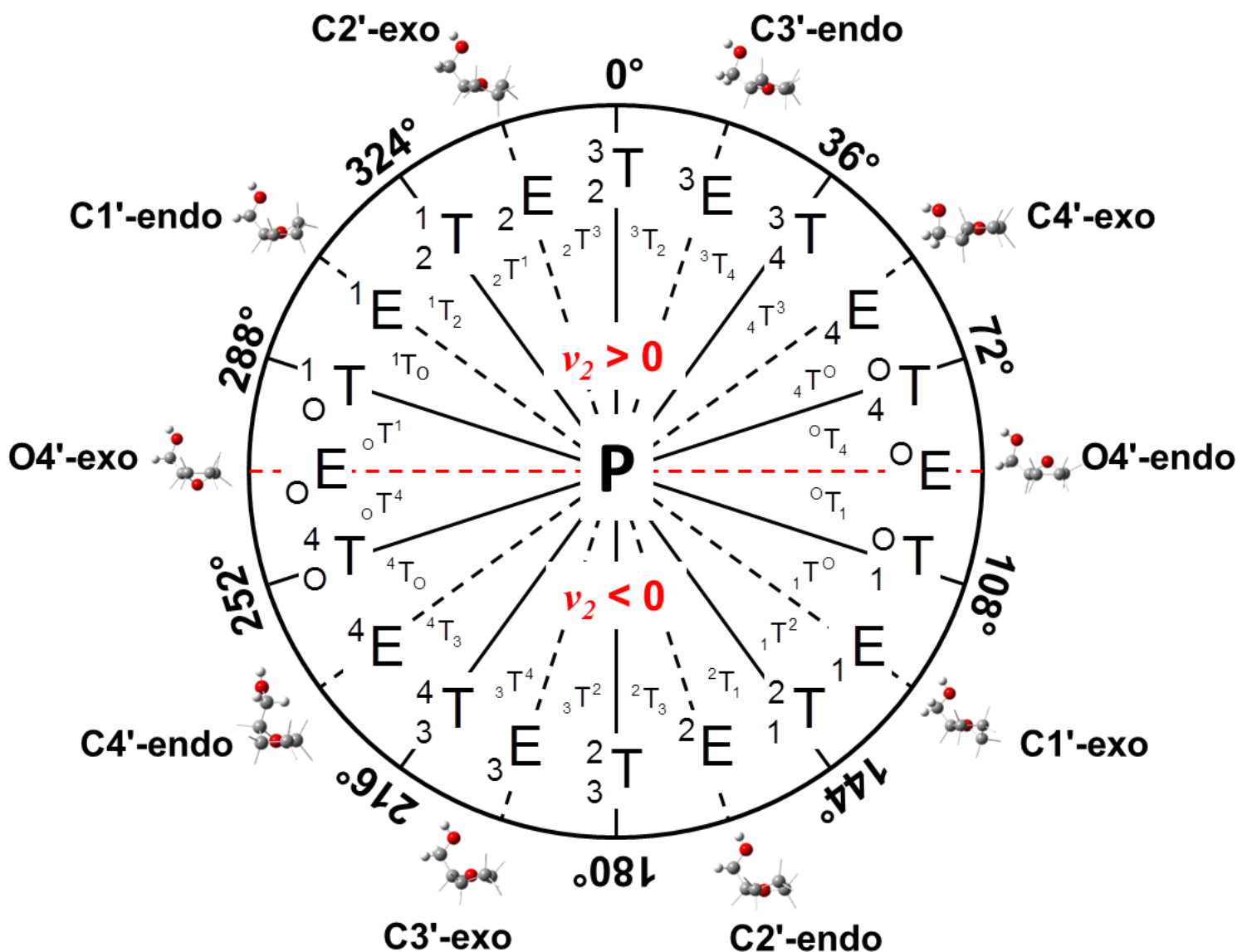
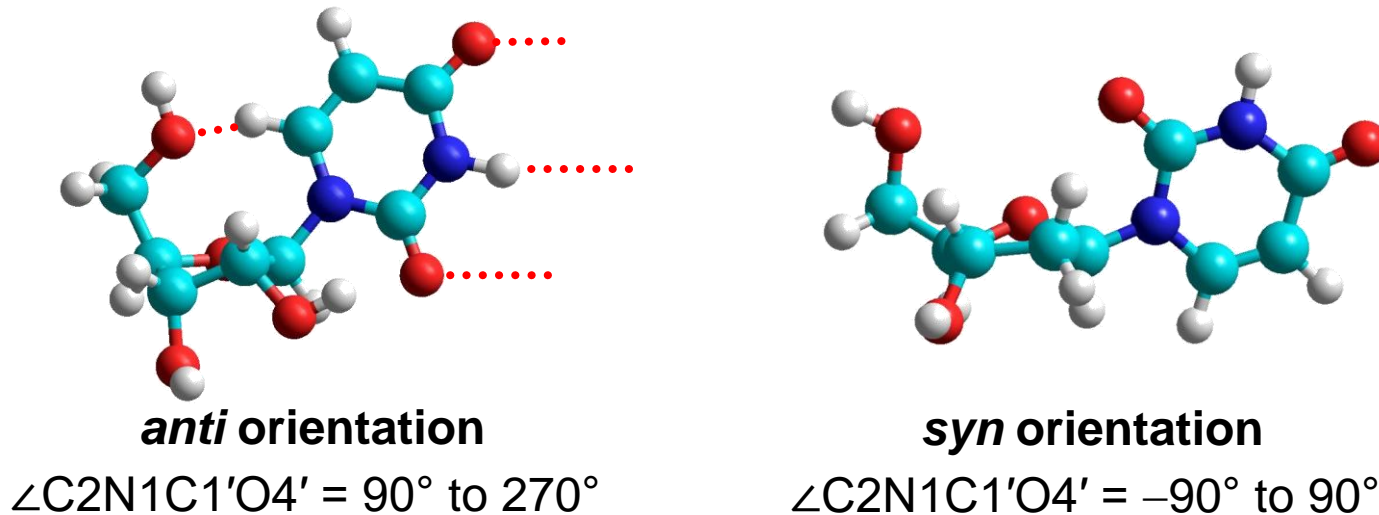


Figure S2.

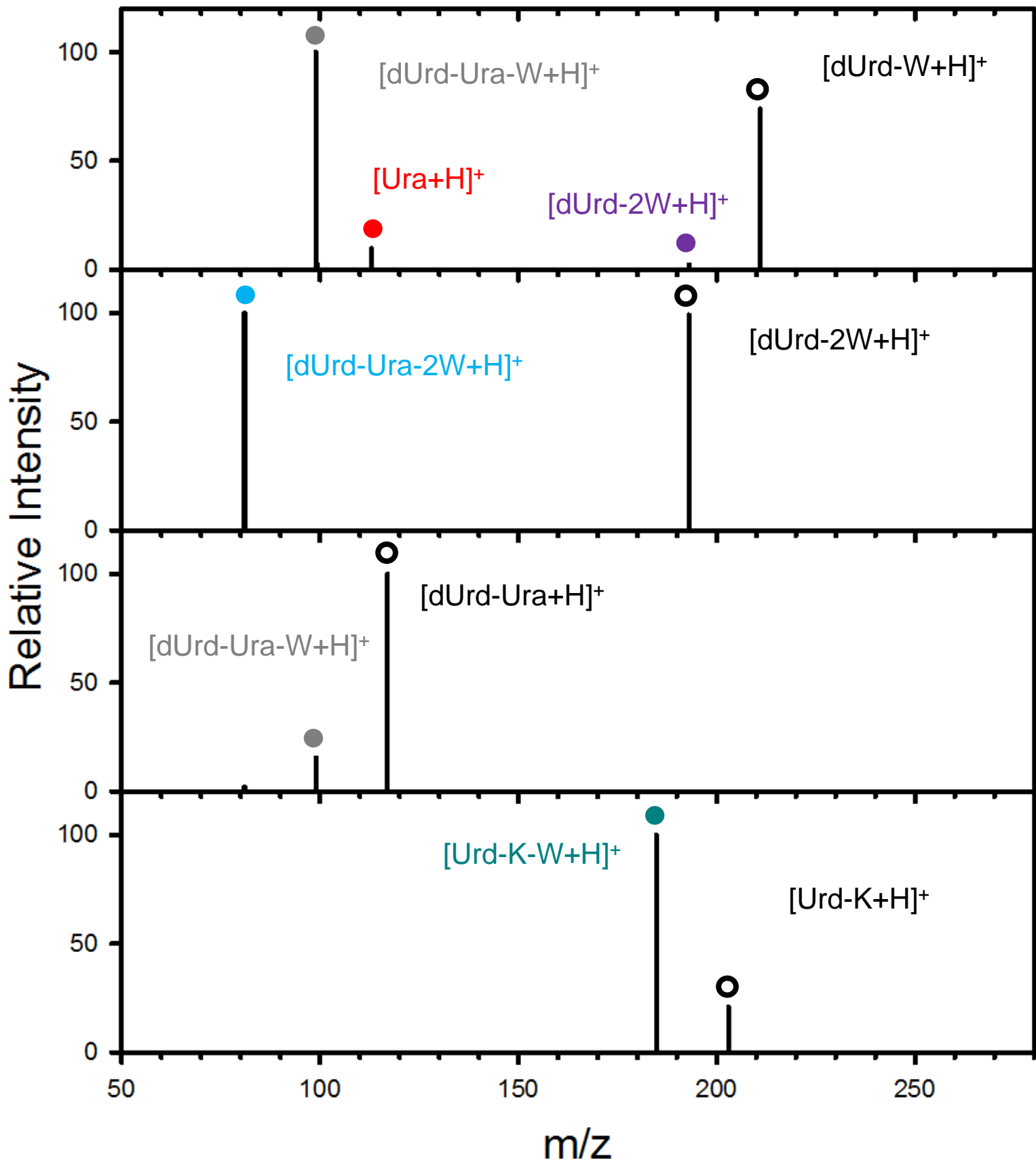


Figure S3.

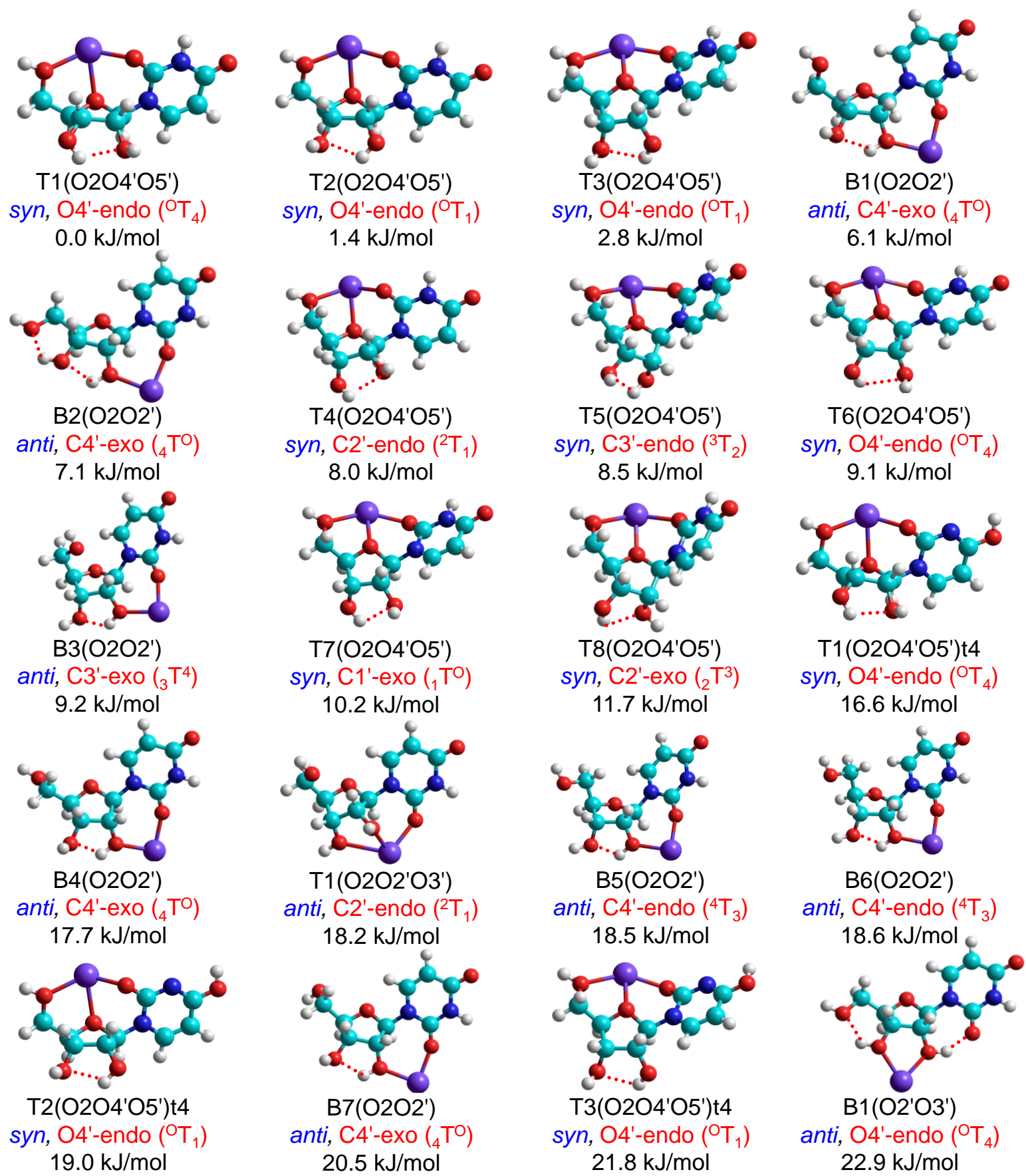
 $[\text{Urd}+\text{Na}]^+$

Figure S3.

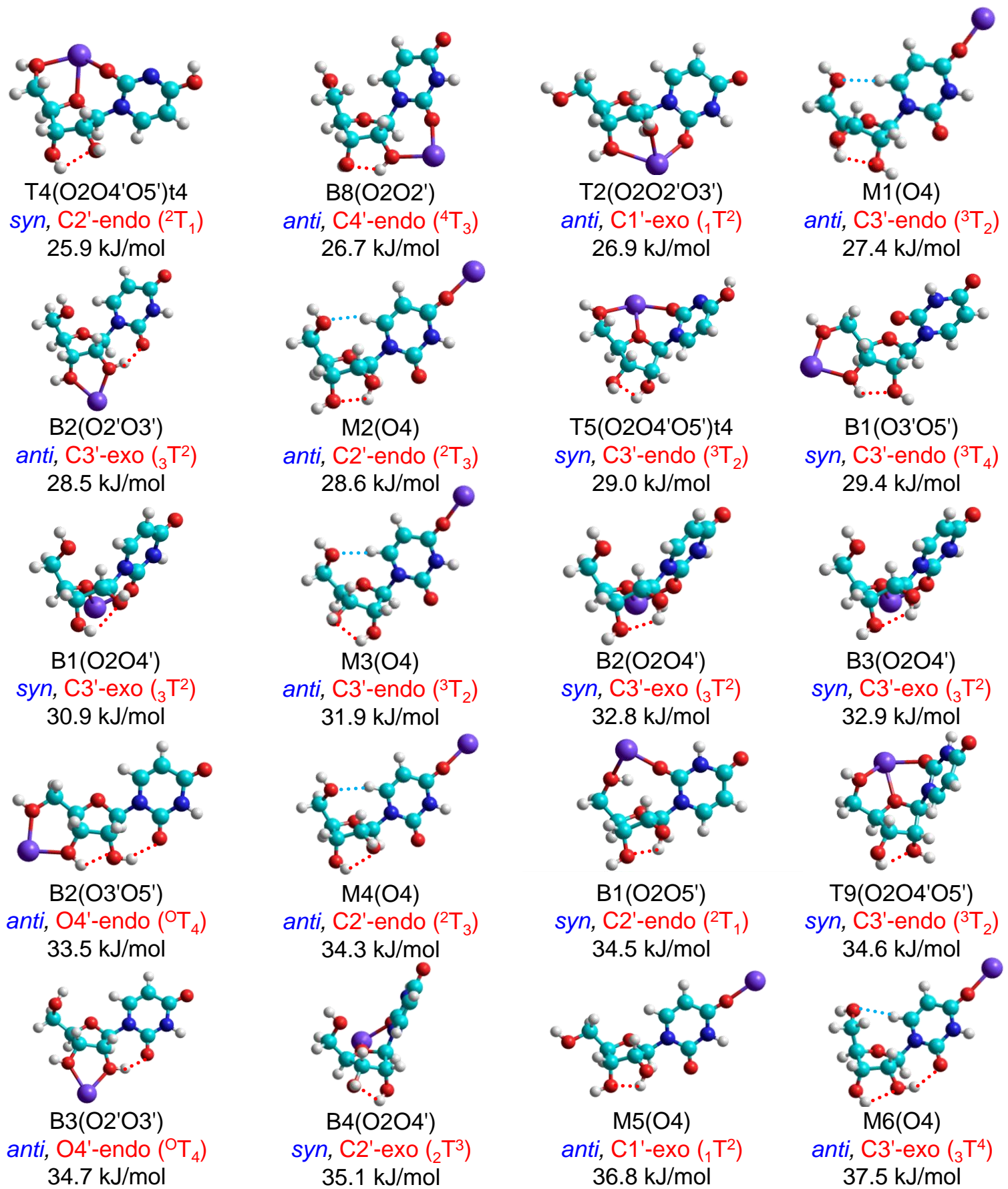
[Urd+Na]⁺

Figure S3.

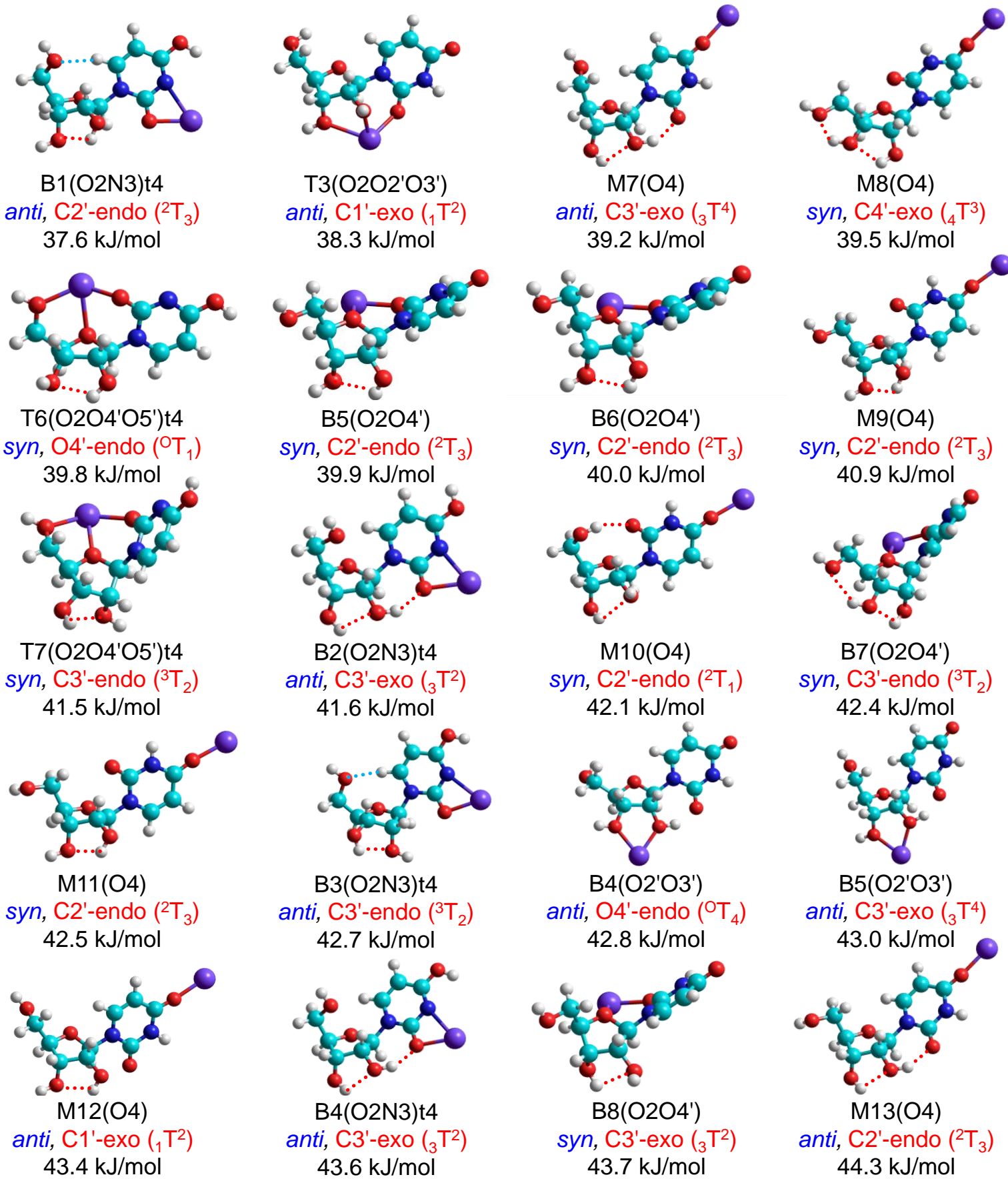
[Urd+Na]⁺

Figure S3.

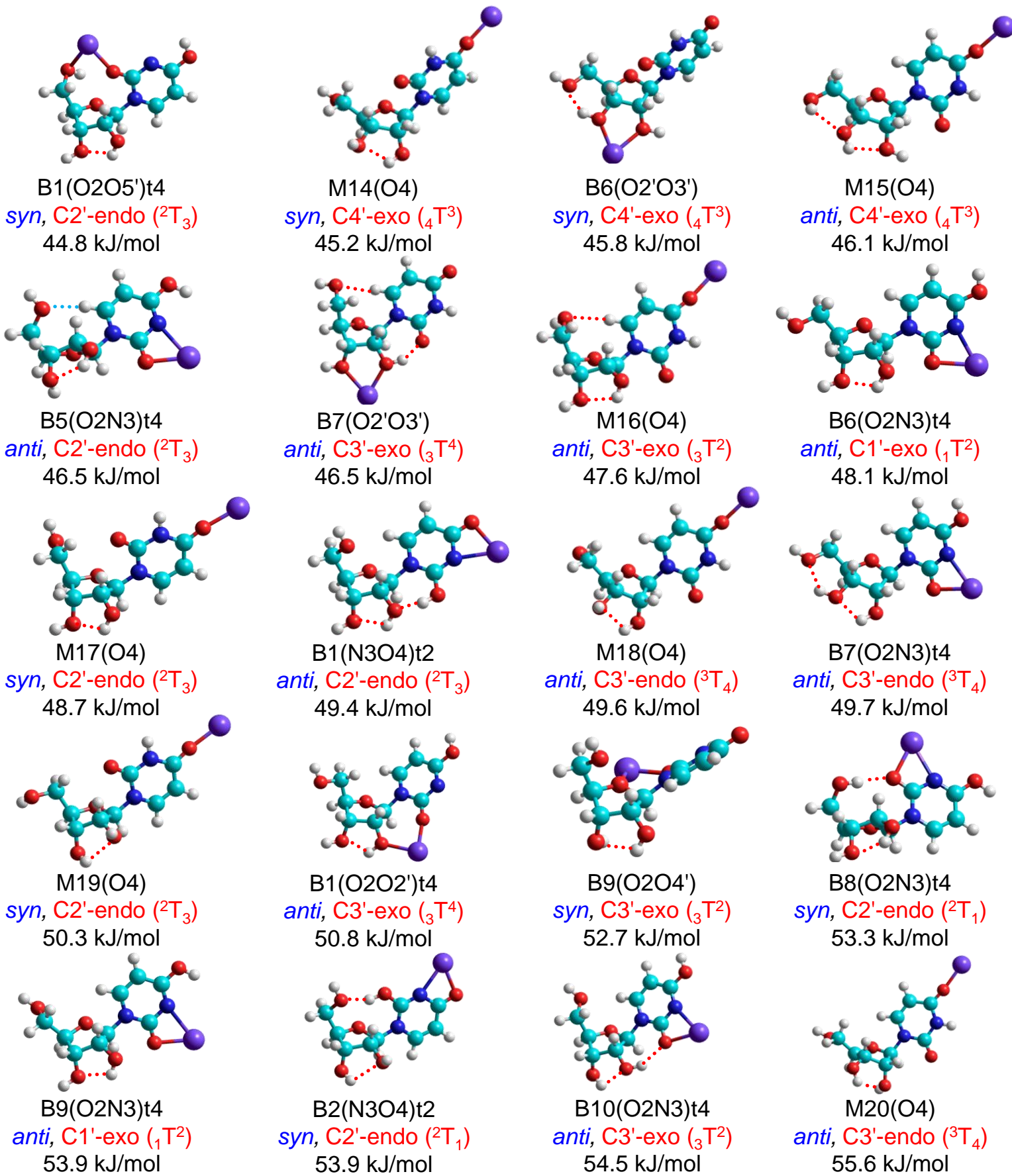
 $[Urd+Na]^+$

Figure S3.

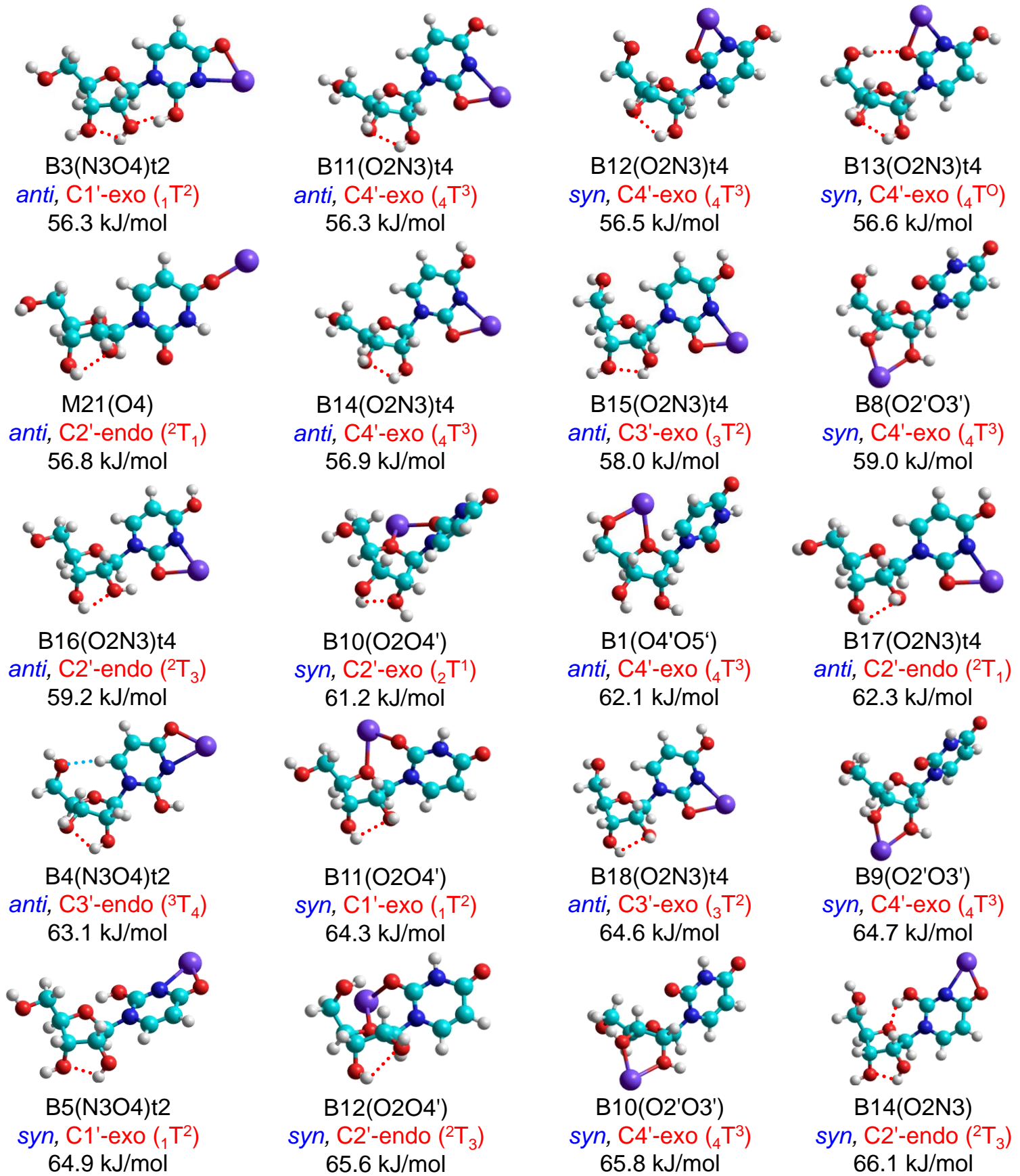
[Urd+Na]⁺

Figure S3.

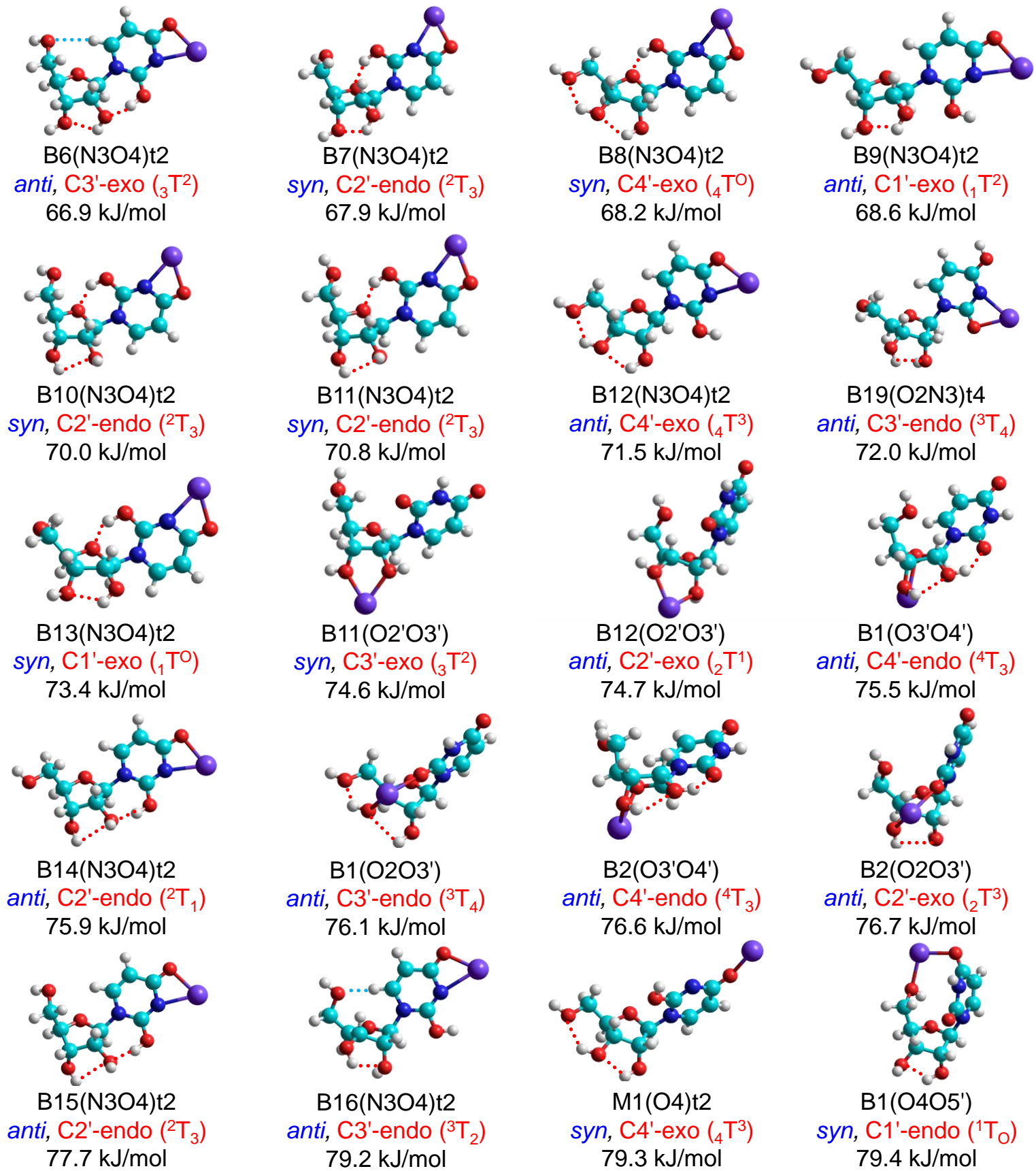
[Urd+Na]⁺

Figure S3.

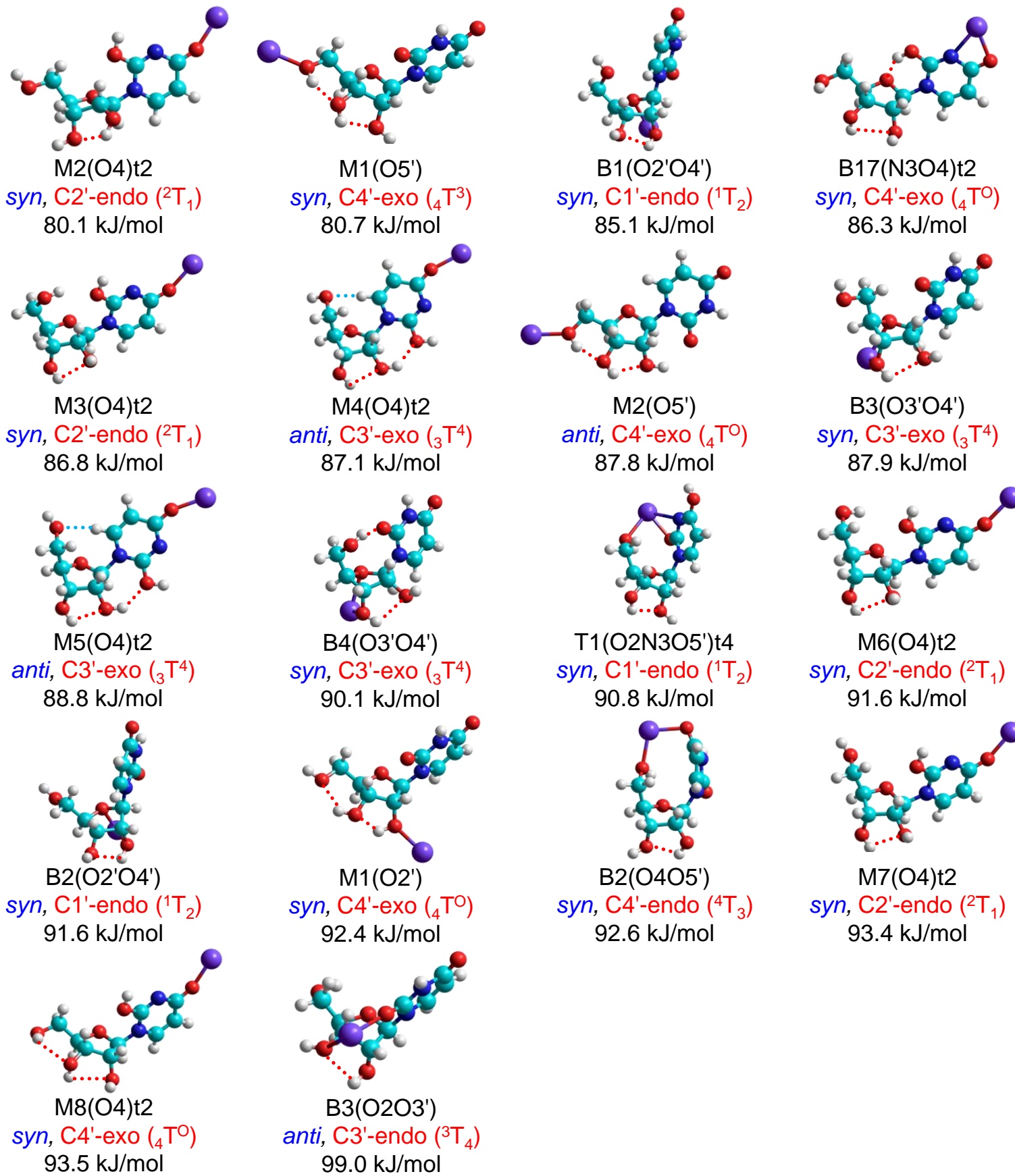
 $[\text{Urd}+\text{Na}]^+$

Figure S4.

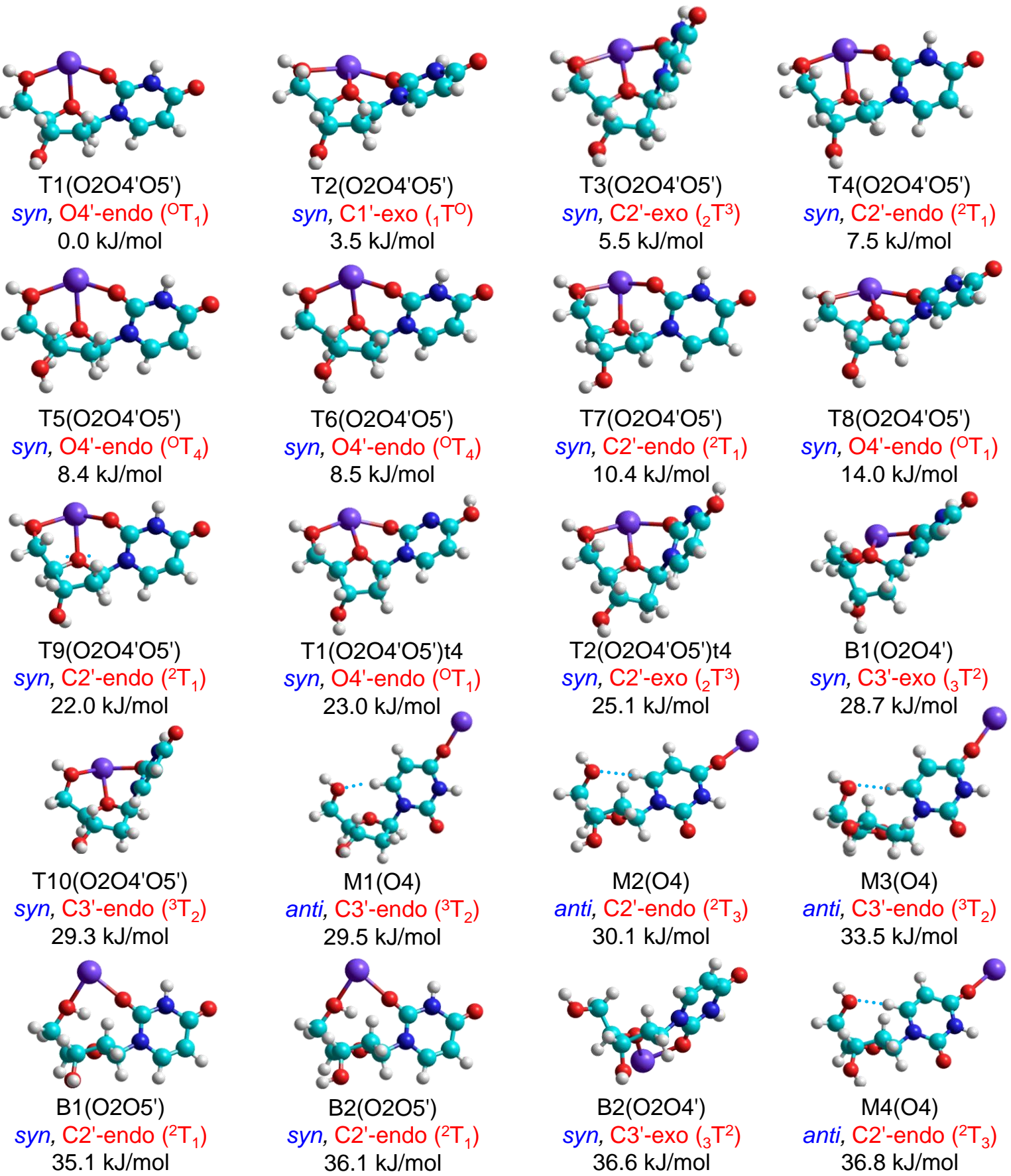
 $[dUrd+Na]^+$

Figure S4.

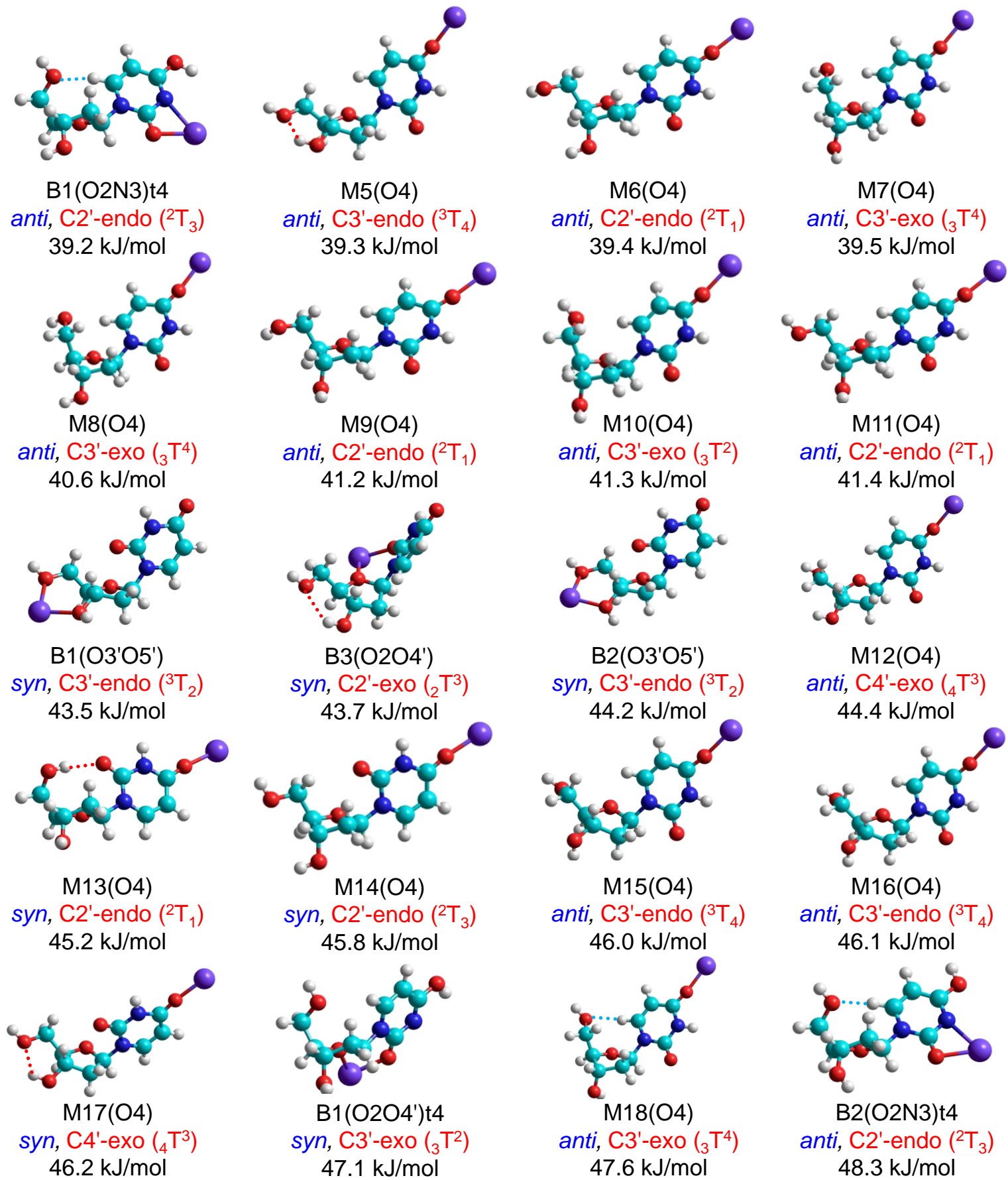
 $[dUrd+Na]^+$

Figure S4.

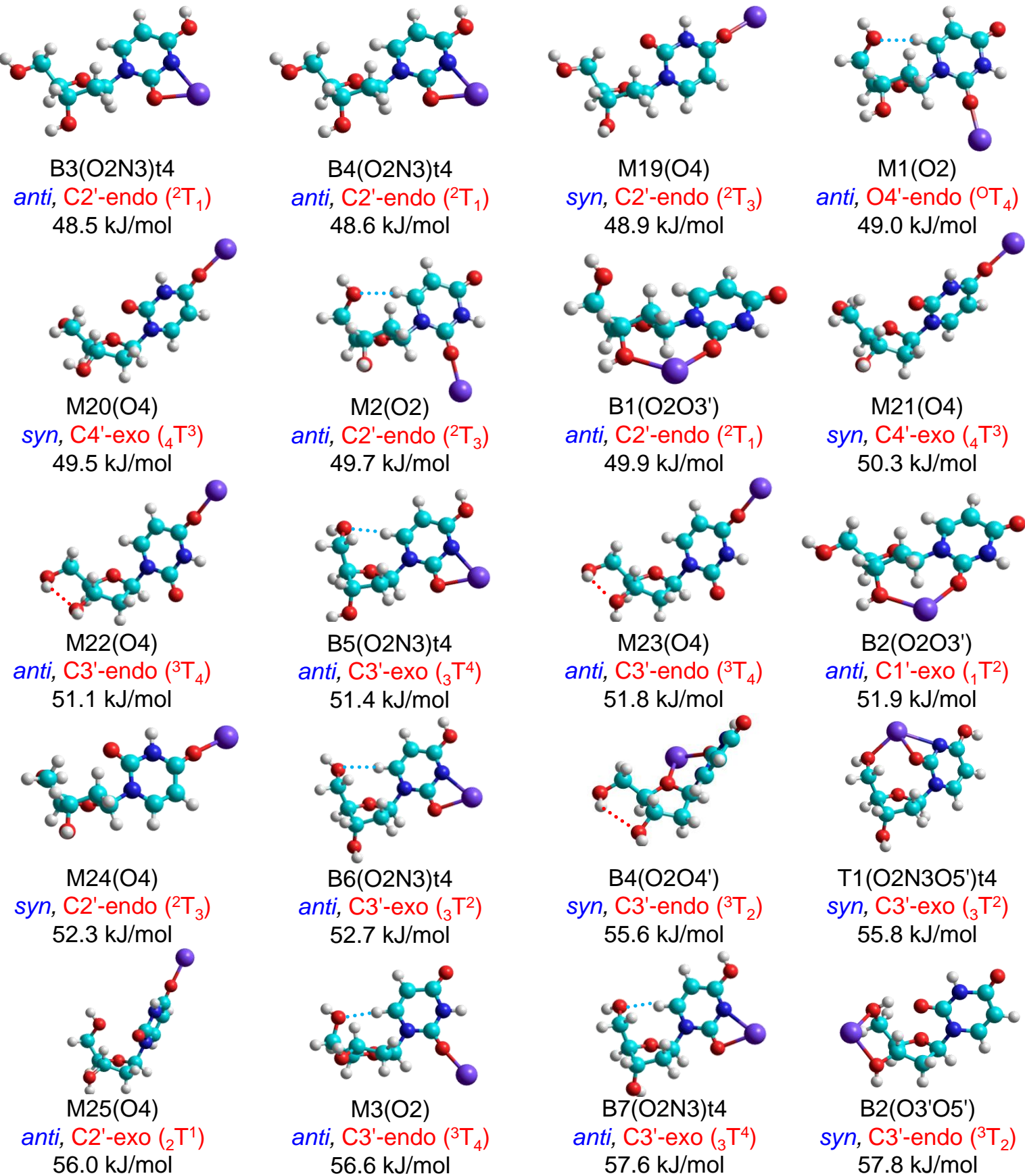
 $[dUrd+Na]^+$

Figure S4.

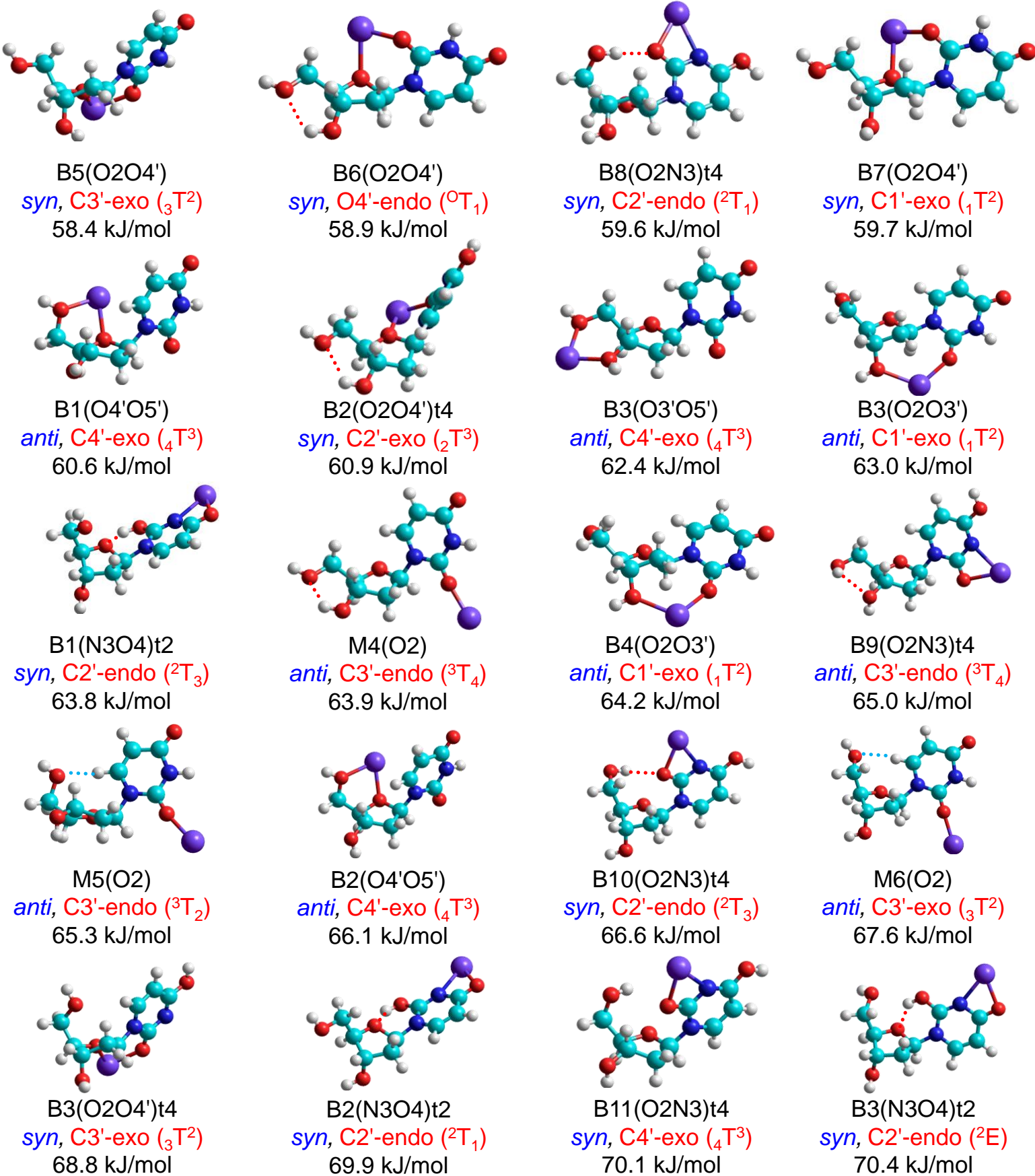
 $[dUrd+Na]^+$

Figure S4.

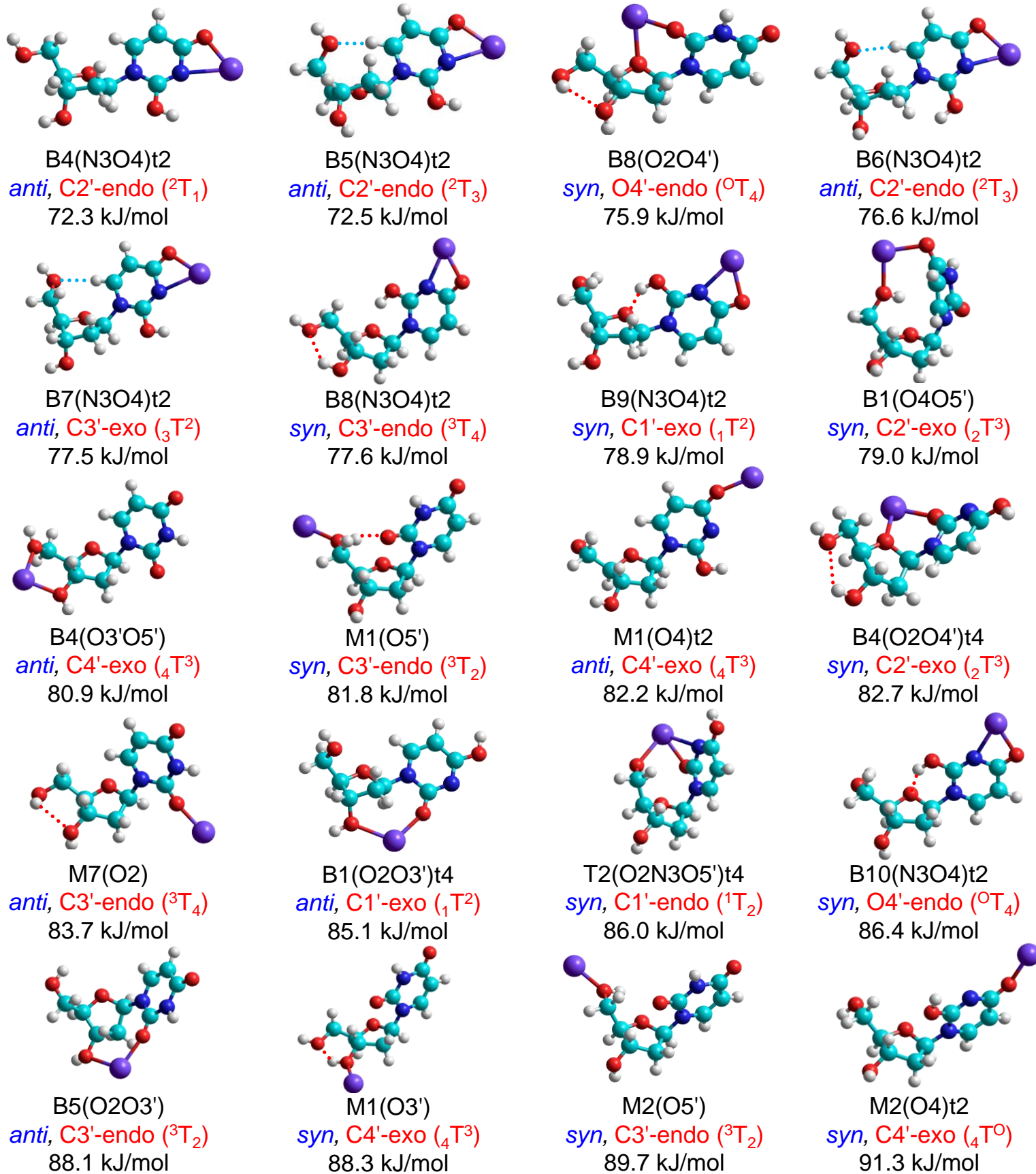
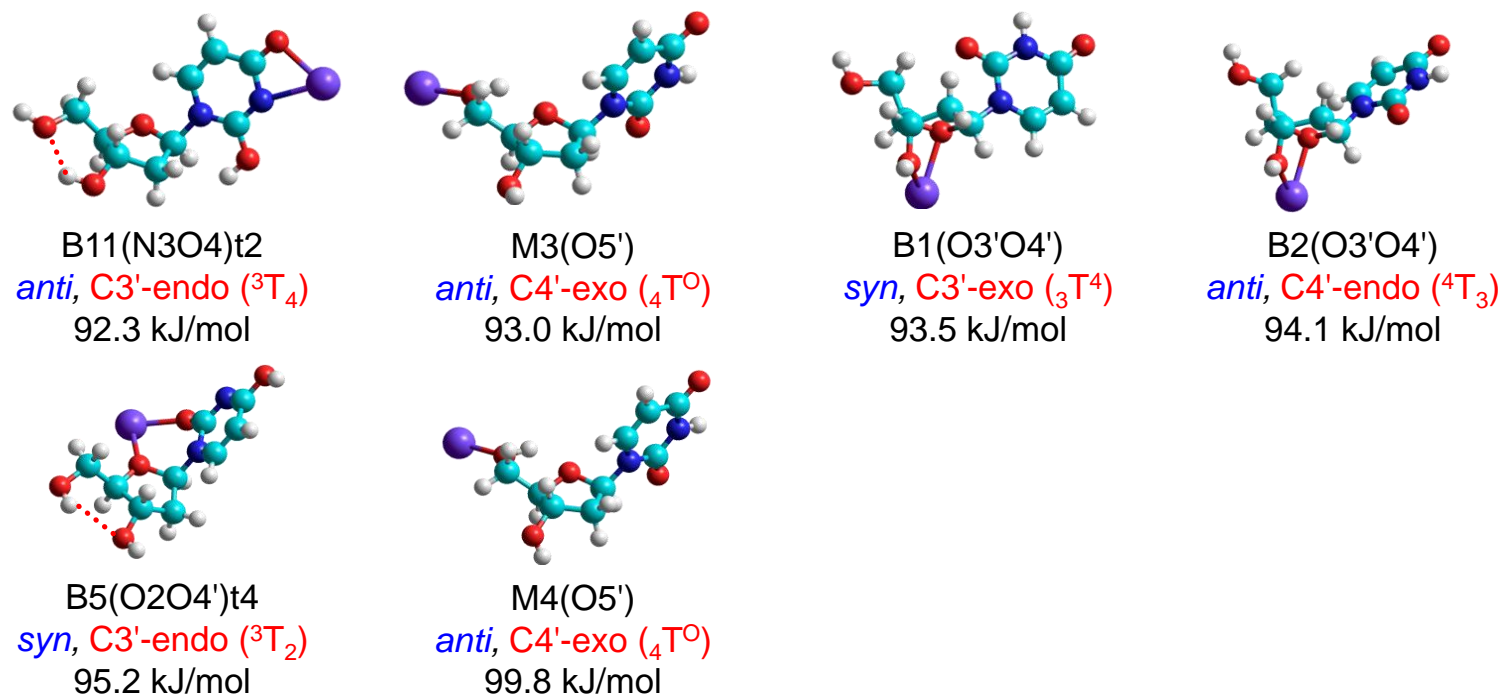
 $[dUrd+Na]^+$

Figure S4.



[dUrd+Na]⁺

Figure S5.

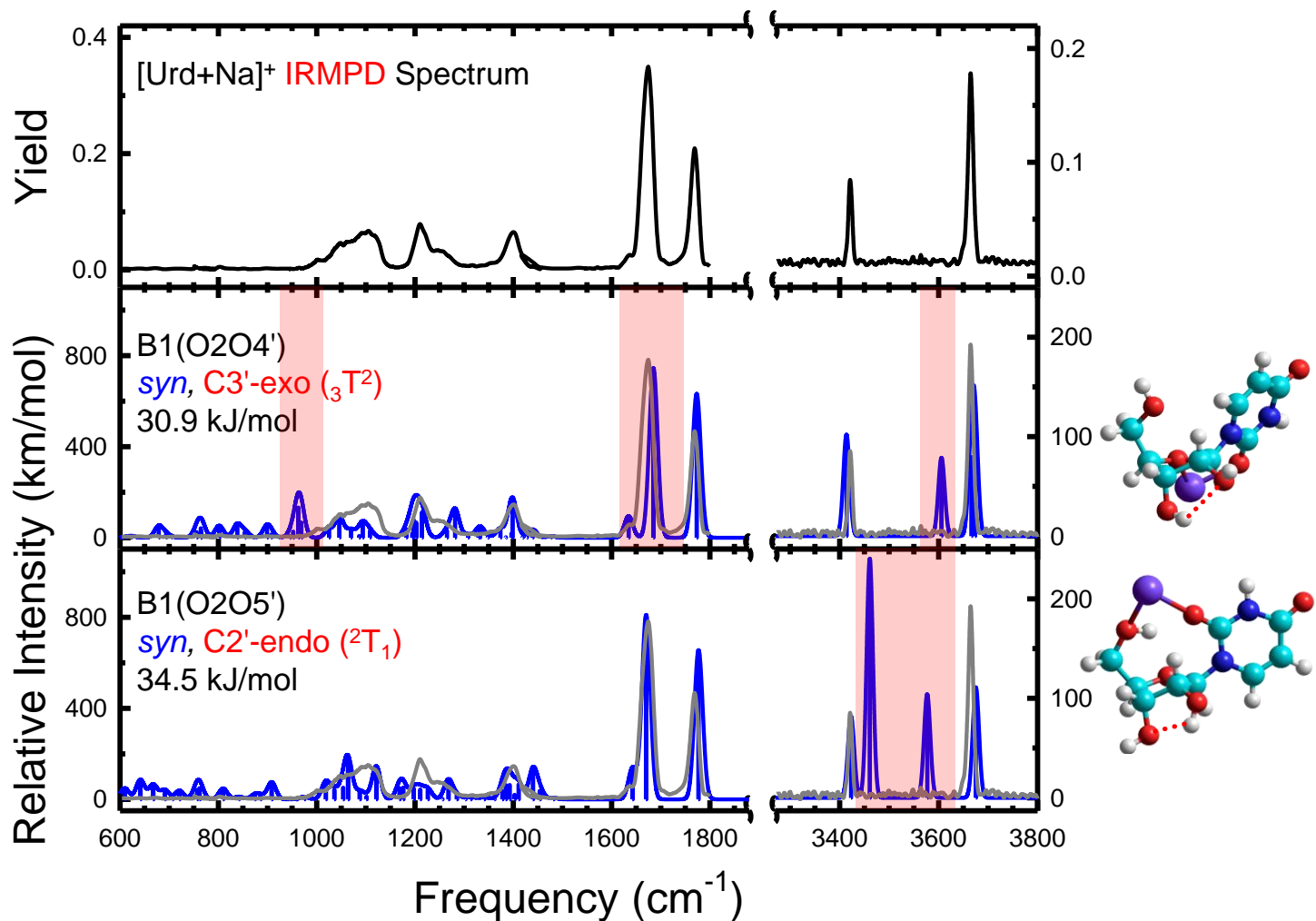


Figure S6.

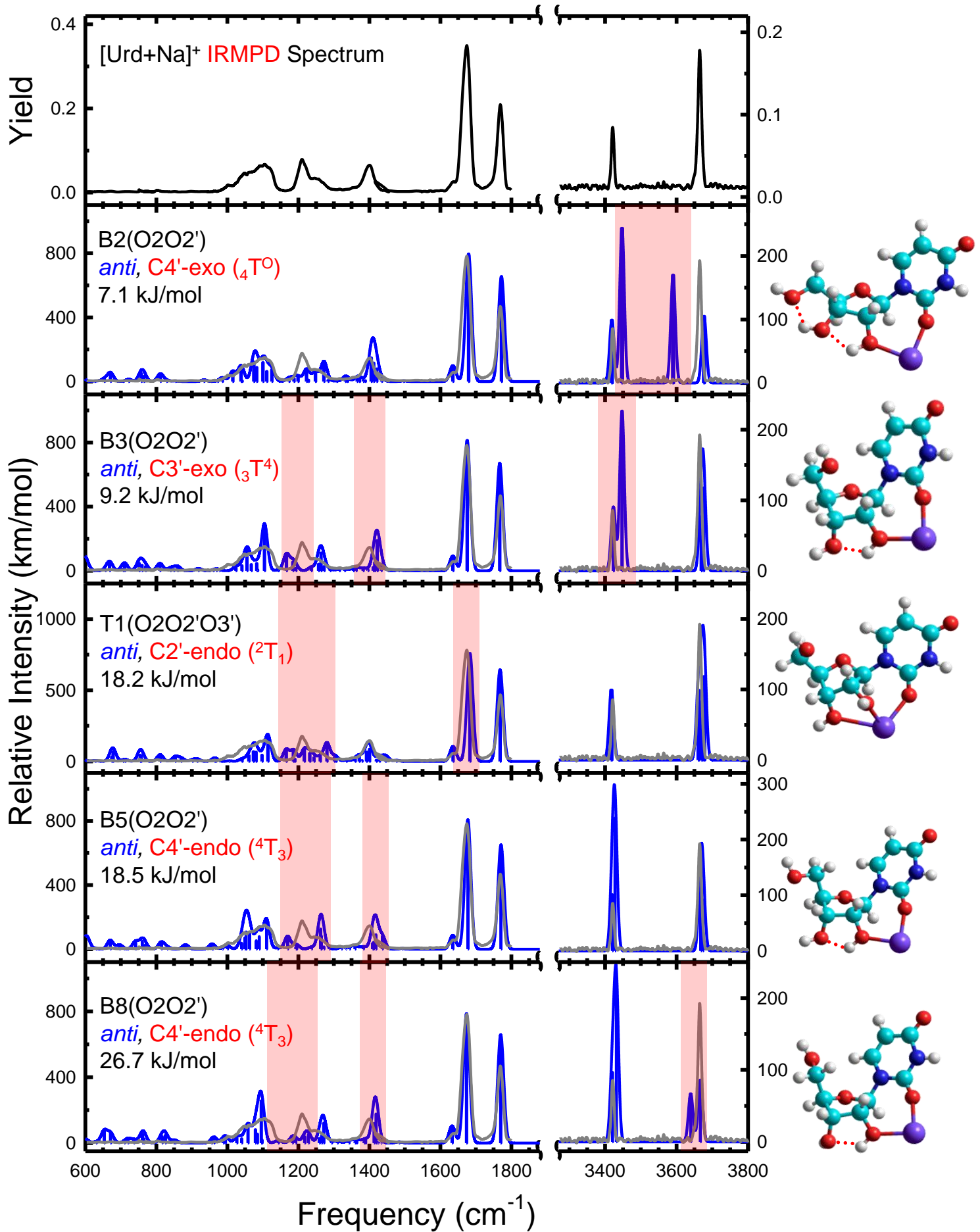


Figure S7.

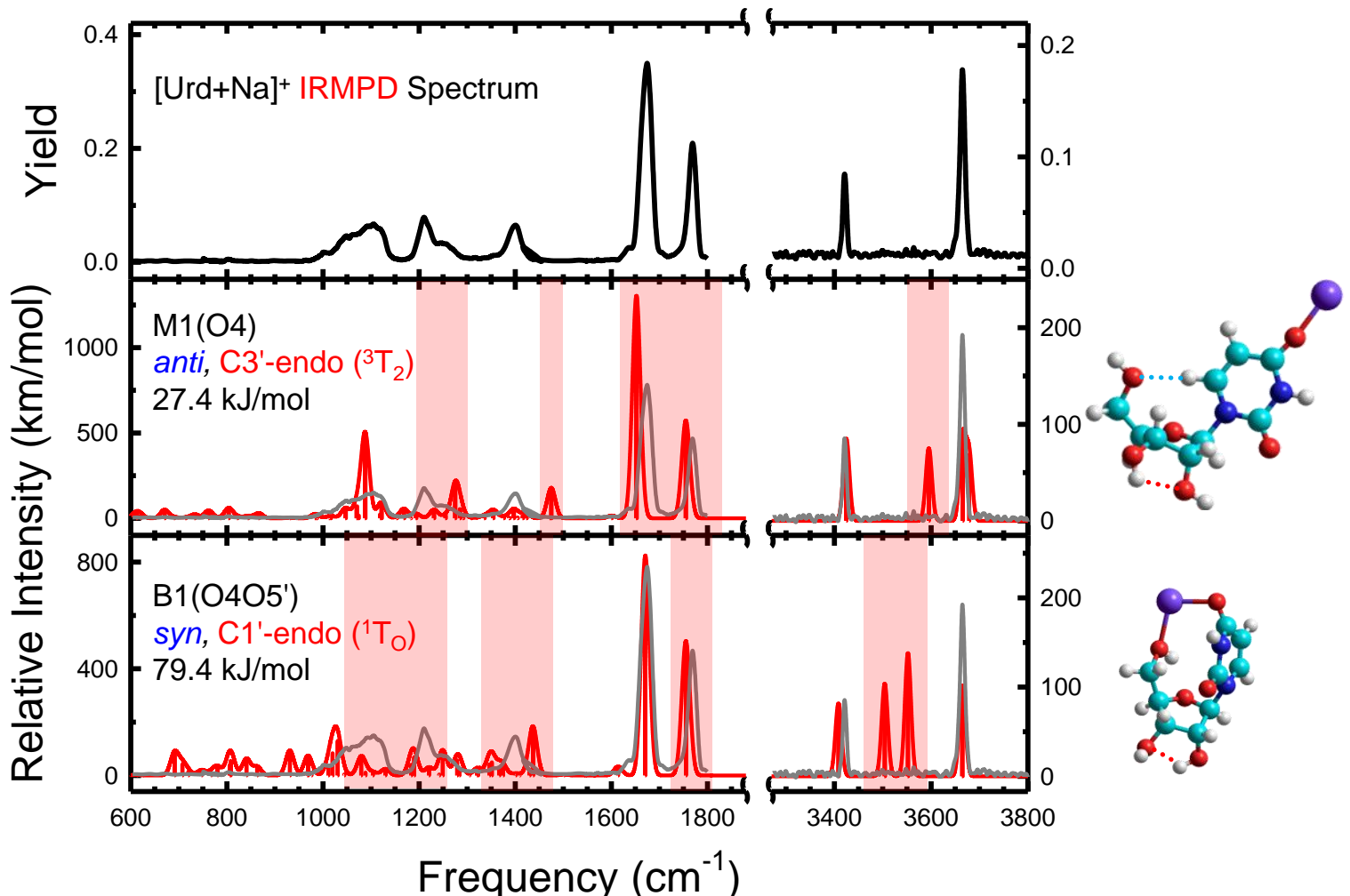


Figure S8.

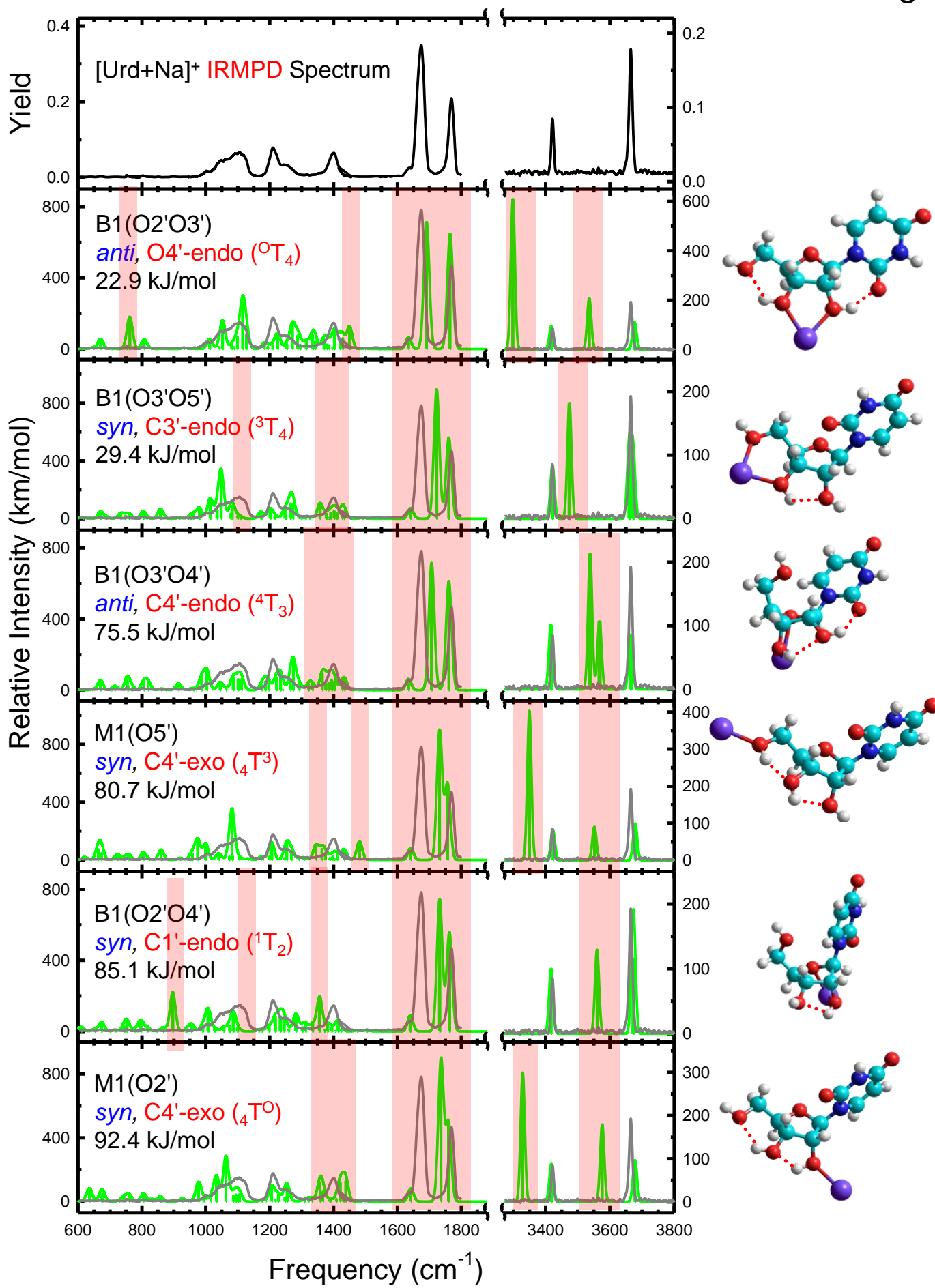


Figure S9.

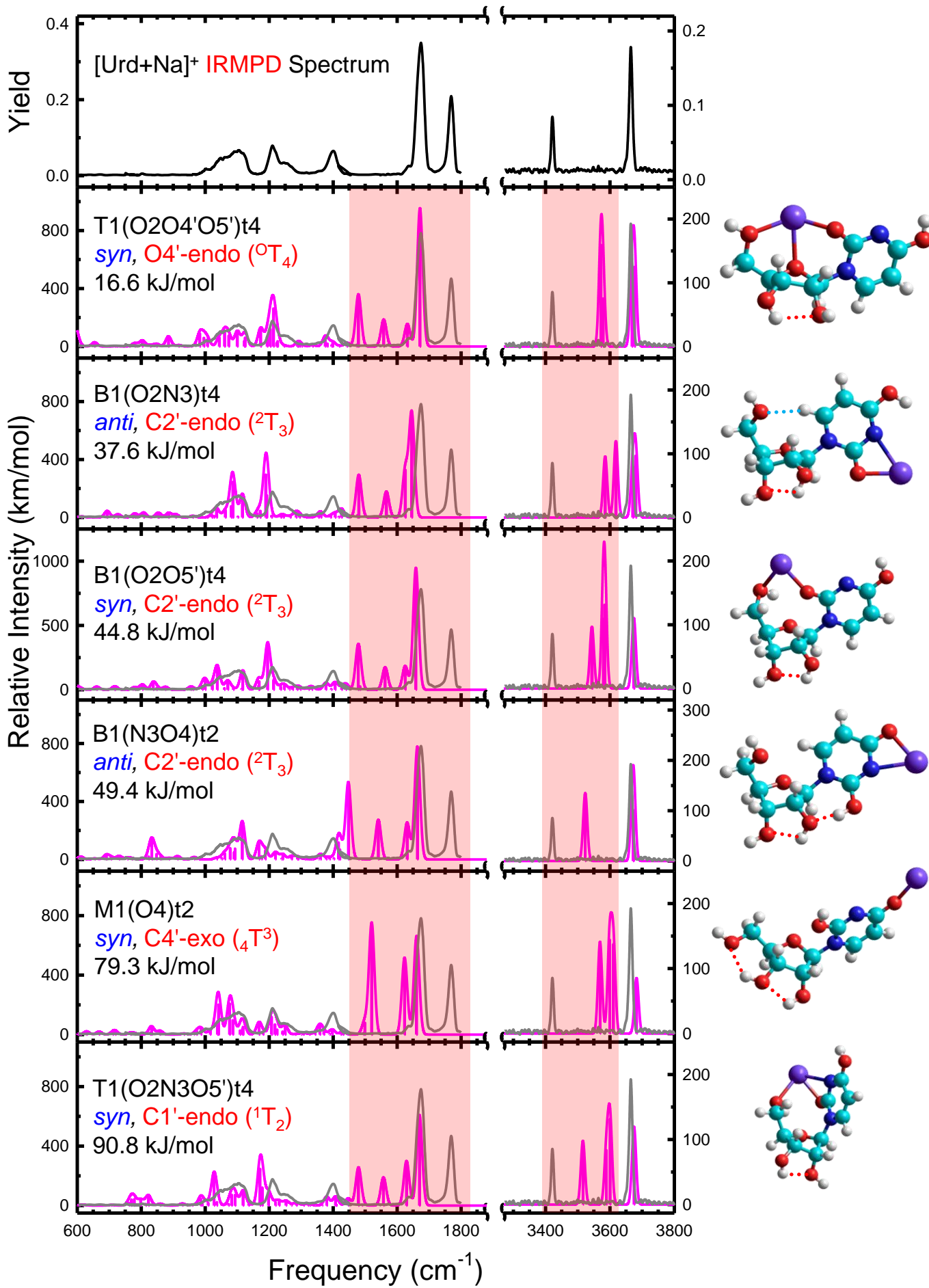


Figure S10.

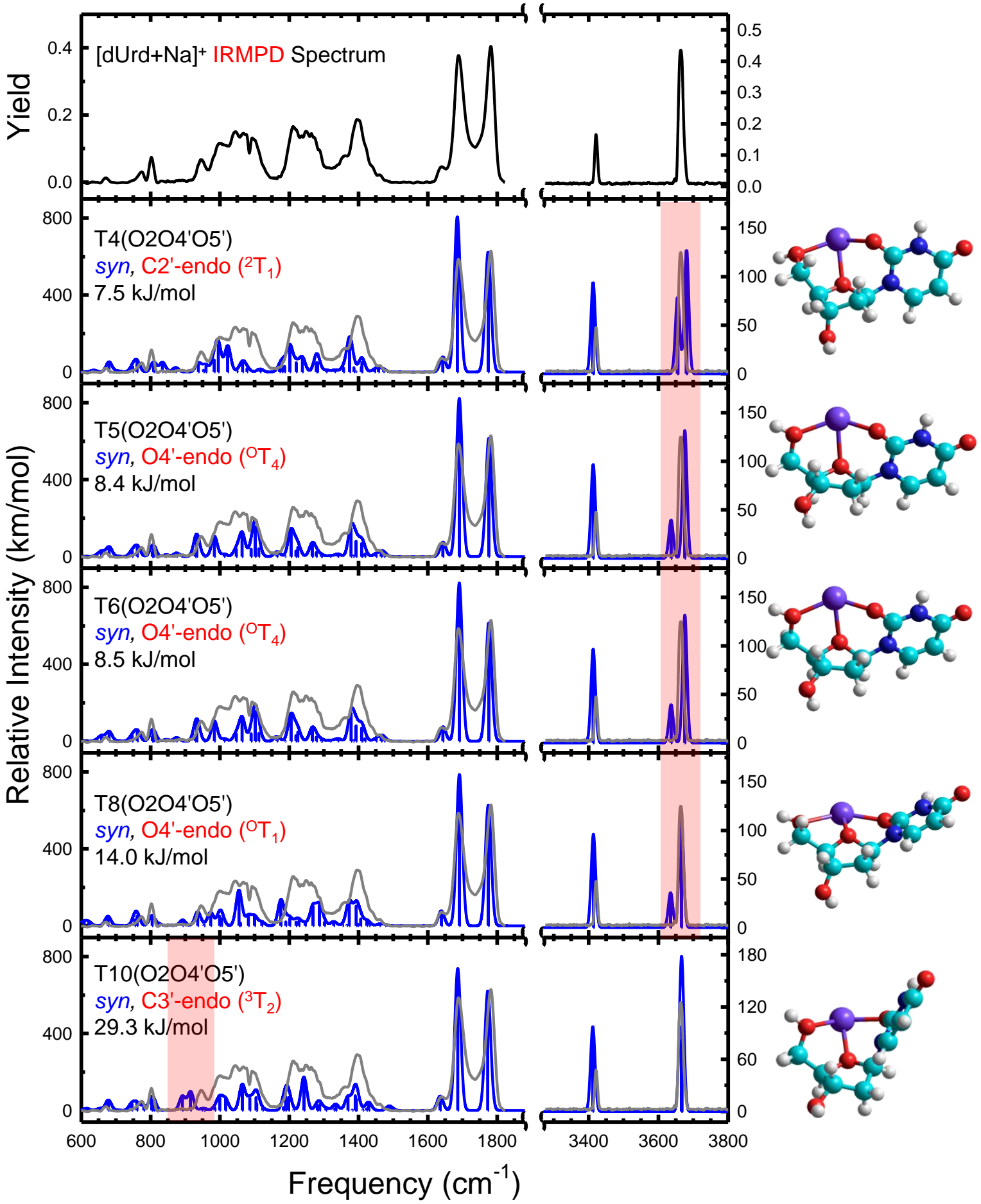


Figure S11.

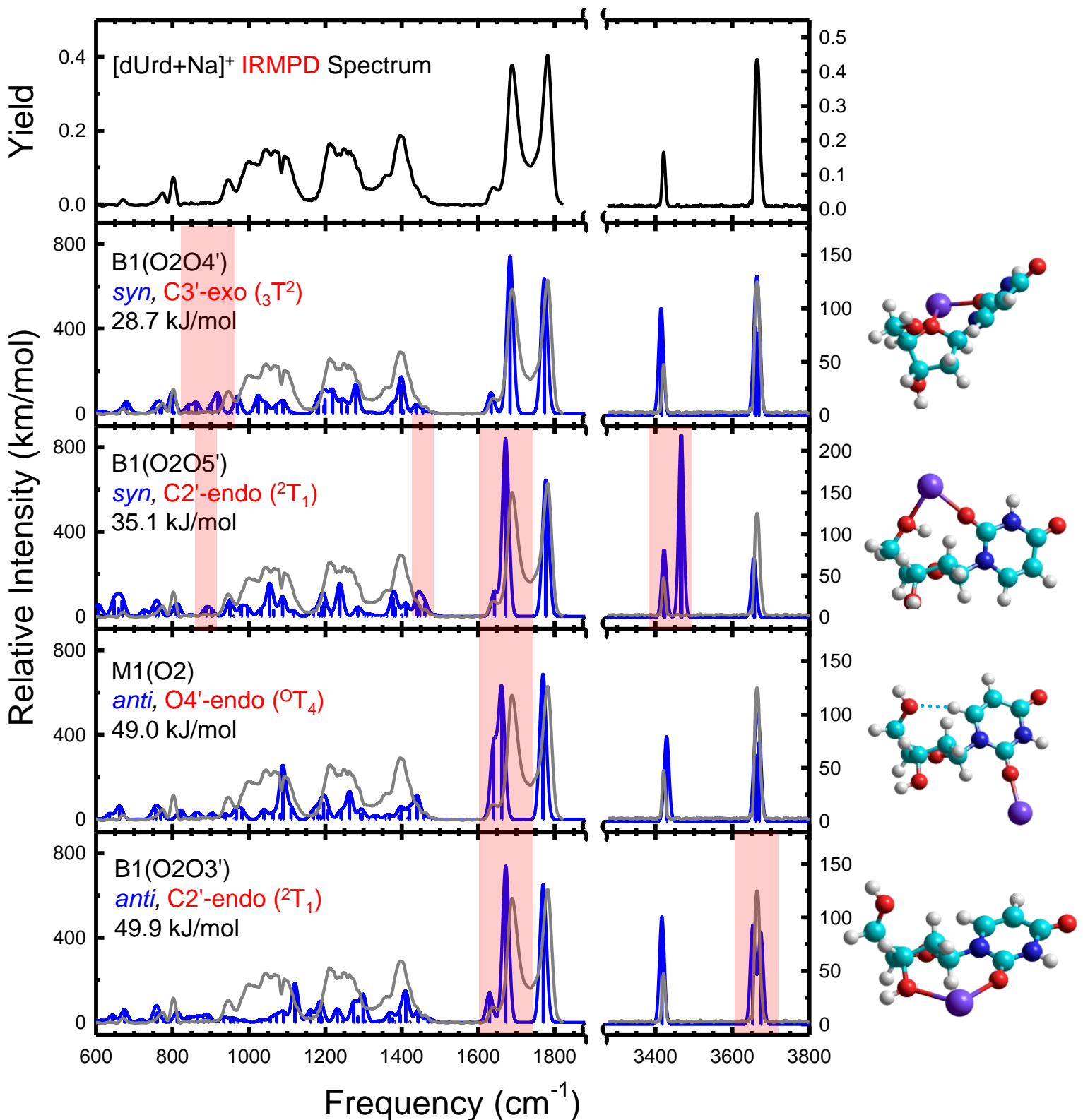


Figure S12.

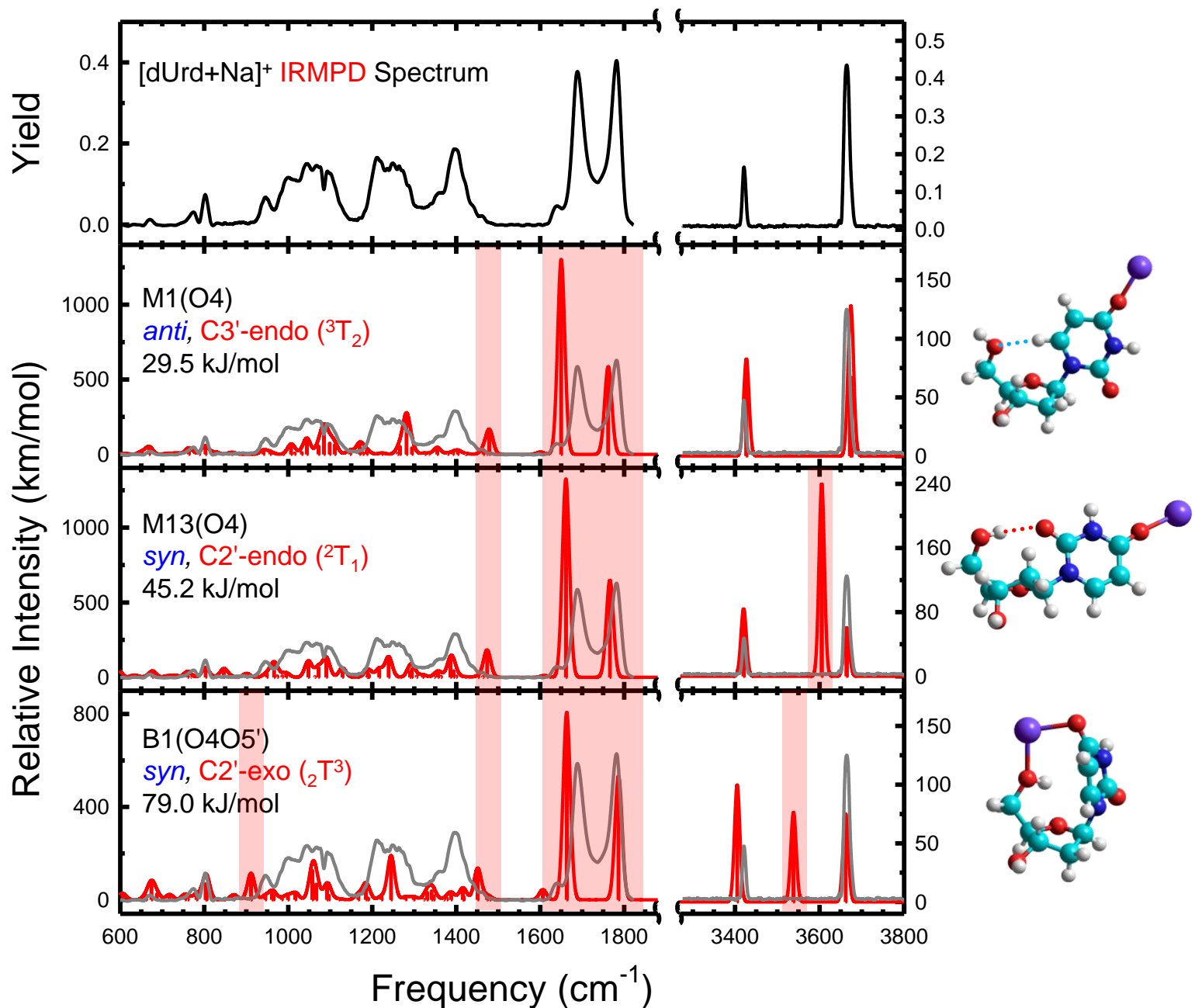


Figure S13.

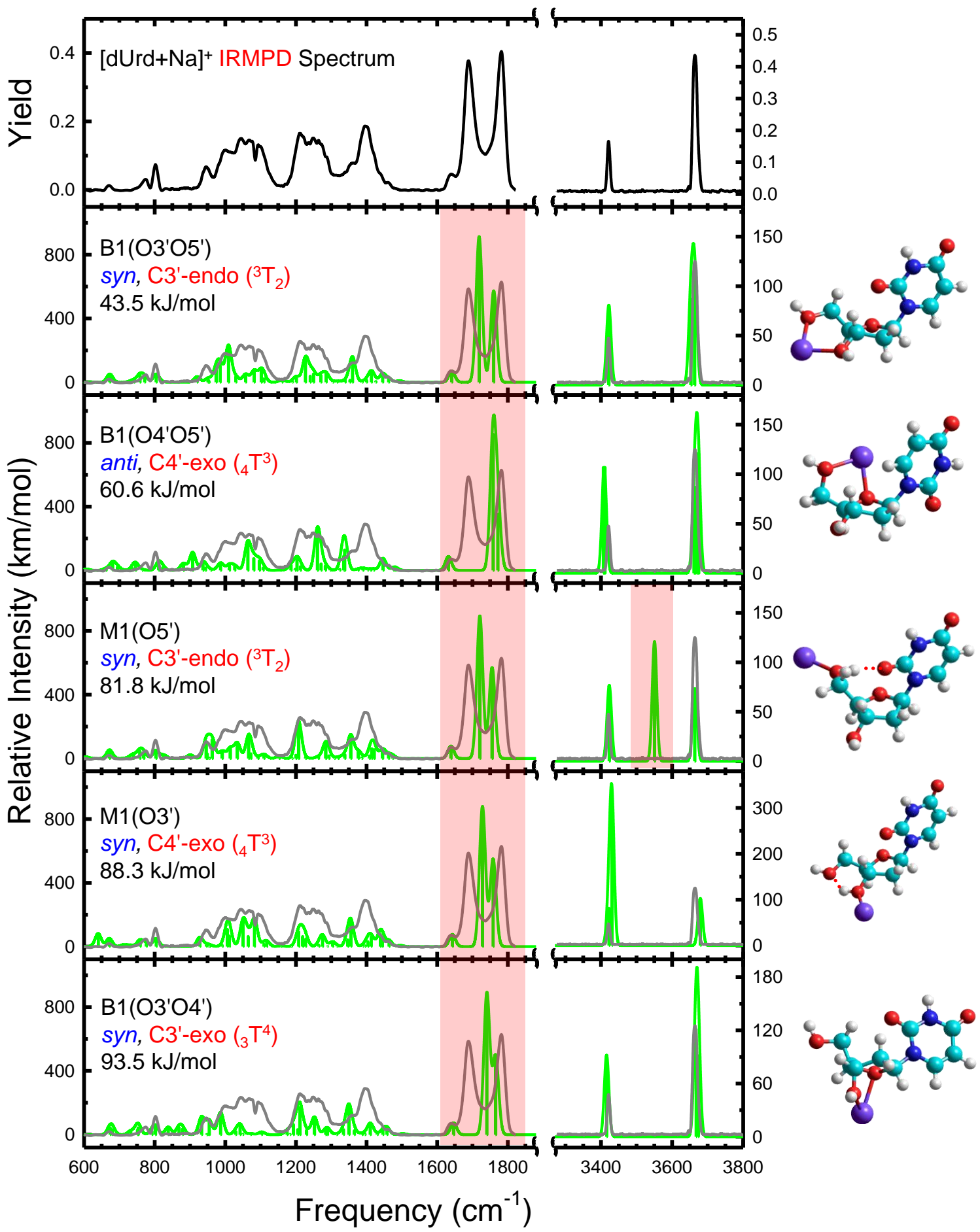


Figure S14.

